Journal of
Materials Chemistry A

Accepted Manuscript

This article can be cited before page numbers have been issued, to do this please use: K. McCombie, E. Wildman, S. Fop, R. Smith, J. Skakle and A. Mclaughlin, *J. Mater. Chem. A*, 2017, DOI: 10.1039/C7TA08989A.

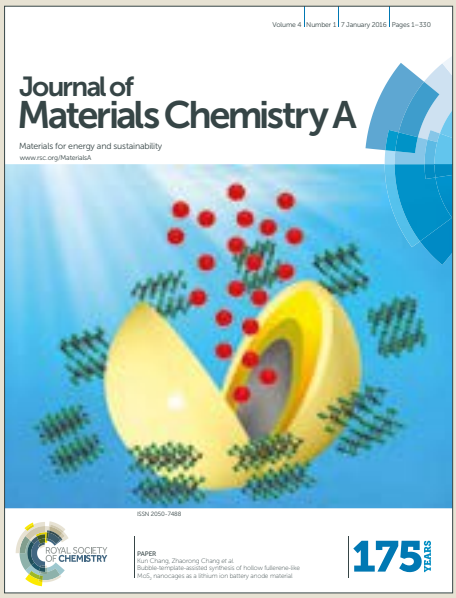

ROYAL SOCIETY OF CHEMISTRY

rsc.li/materials-a

View Article Online
DOI: 10.1039/C7TA08989A

Journal of Materials Chemistry A

ARTICLE

The Crystal Structure and Electrical Properties of the Oxide Ion Conductor $Ba_3WNbO_{8.5}$

Received 00th January 20xx,
Accepted 00th January 20xx

DOI: 10.1039/x0xx00000x

www.rsc.org/

K. S. McCombie [a], E. J. Wildman [a], S. Fop [a], R. I. Smith [b], J. M. S. Skakle [a] and A. C. Mclaughlin [a]

The structural and electrical properties of the hexagonal perovskite derivative $Ba_3WNbO_{8.5}$ have been investigated. $Ba_3WNbO_{8.5}$ crystallises in a hybrid of the 9R hexagonal perovskite and palmierite structure as recently reported for the novel oxide ion conductor $Ba_3MoNbO_{8.5}$. $Ba_3WNbO_{8.5}$ is also an oxide ion conductor and appears to exhibit oxide ionic conduction with negligible electronic conductivity over a wider pO_2 range than $Ba_3MoNbO_{8.5}$. A neutron diffraction study has revealed that at 20 °C the average structure of $Ba_3WNbO_{8.5}$ contains just 13 % of $W(1)/Nb(1)O_4$ tetrahedra within the average structure of $Ba_3WNbO_{8.5}$ in comparison to 50% of $Mo(1)/Nb(1)O_4$ tetrahedra in $Ba_3MoNbO_{8.5}$. The presence of $(M/Nb)O_4$ tetrahedra with non-bridging apical oxygen atoms is an important prerequisite for the ionic conduction observed in the $Ba_3MNbO_{8.5}$ system (M = W, Mo). The strong reduction in the ratio of $(M/Nb)O_4$ tetrahedra to $(M/Nb)O_6$ octahedra upon replacement of W^{6+} for Mo^{6+} results in a reduction in the ionic conductivity by an order of magnitude at 450 °C. The bulk conductivities converge upon heating so that at 600 °C the bulk conductivity of $Ba_3WNbO_{8.5}$, σ_b = 0.0017 S cm^{-1}, is comparable to that of $Ba_3MoNbO_{8.5}$ (σ_b = 0.0022 S cm^{-1}). The results demonstrate that other members of the $Ba_3MM'O_{8.5}$ family can support oxide ion conductivity and further studies of hexagonal perovskite derivatives are warranted.

Introduction

There has been increasing interest in oxide ion conductors in recent years due to their application in oxygen sensors, oxygen separation membranes and as electrolytes in solid oxide fuel cells (SOFCs). [1-4] The development of SOFCs as alternative systems for the generation of electric power is important due to their advantages over conventional methods of power generation, including significantly higher efficiencies of energy conversion, achieving efficiencies of greater than 85% for combined heat and power (CHP) applications. [5, 6] In addition, SOFCs have the advantage of fuel flexibility, are extremely reliable and are more environmentally friendly, producing reduced emissions of pollutants such as CO_2 and NO_x gases. [7]

A variety of materials that exhibit oxide ion conductivity have been reported, including fluorite-related structures, [4, 8], $La_2Mo_2O_9$ (LAMOX) based materials [9], Bi_2O_3 and $Bi_4V_2O_{11}$ based oxides, [10] germanate apatite oxide systems [11], perovskites such as strontium and magnesium doped lanthanum gallates (LSGM) [12], $Na_{0.5}Bi_{0.5}TiO_3$ (NBT) [13] and the perovskite derivative $NdBaInO_4$. [14] The major challenge in the commercialisation of SOFC technology has been the high temperature of operation (800 - 1000 °C) required to achieve sufficient conductivities from conventional zirconia-based electrolytes. [15] The use of such high temperatures leads to slow start-up times, thermal degradation over time and necessitates the use of expensive materials. [16] Reducing the operating temperature of the SOFC to an intermediate range (400 – 600 °C) would reduce costs, shorten start-up times, widen the choice of materials used in the fuel cell and extend the lifetime of the SOFC. [17] As a result there is increasing interest in the development of electrolyte materials with sufficiently high oxide ion conductivities at lower temperatures. It is therefore important to discover and characterise new classes of oxide ion conducting materials.

Recently we have reported a novel oxide ion conductor, $Ba_3MoNbO_{8.5}$ [18]. $Ba_3MoNbO_{8.5}$ is the first hexagonal perovskite derivative reported to exhibit significant oxide ion conductivity and has a bulk conductivity of 2.2 x 10^{-3} S cm^{-1} at 600 °C, comparable to that of conventional SOFC electrolyte materials. $Ba_3MoNbO_{8.5}$ exhibits oxygen transport numbers of 0.99 in air/O_2 and 0.92 in air/5% H_2 in Ar at 600 °C, suggesting that $Ba_3MoNbO_{8.5}$ is an oxide ion conductor with negligible electronic conductivity in air/O_2 and that a small amount of electronic conduction is observed in air/5% H_2 in Ar. [18] $Ba_3MoNbO_{8.5}$ crystallises in a hybrid of the 9R hexagonal perovskite and palmierite structure. The crystal structure contains Mo/NbO_x in a mixture of octahedral and tetrahedral coordination geometry and has intrinsic oxygen vacancies. [18] $Ba_3MoNbO_{8.5}$ presents an unusual structural rearrangement upon increasing the temperature which is caused by modification of the oxygen/vacancy distribution on the

[a] Department of Chemistry, University of Aberdeen, Meston Walk, Aberdeen AB24 3UE, United KingdomAddress here.
[b] ISIS Facility, STFC Rutherford Appleton Laboratory, Harwell Campus, Didcot, OX11 0QX, UK

Electronic Supplementary Information (ESI) available: [details of any supplementary information available should be included here]. See DOI: 10.1039/x0xx00000x

View Article Online
DOI: 10.1039/C7TA08989A

pseudo-cubic layers [19]. The change in the O(2) and O(3) site populations leads to the concomitant increase of the ratio of $(Mo/Nb)O_4$ tetrahedra to $(Mo/Nb)O_6$ octahedra and enhances the oxide ionic conductivity.

Here, the crystal structure and electrical properties of the novel tungsten derivative $Ba_3WNbO_{8.5}$ are reported. The material $Ba_3WNbO_{8.5}$ also crystallises in a hybrid structure which is intermediate between that of the 9R-polytype and palmierite structures and exhibits oxide ionic conduction with negligible electronic conductivity over a wider pO_2 range than $Ba_3MoNbO_{8.5}$.

Experimental

$Ba_3WNbO_{8.5}$ was prepared by the solid-state reaction of stoichiometric amounts of the starting materials $BaCO_3$ (99.98 %, Sigma-Aldrich), WO_3 (99.9 %, Sigma-Aldrich) and Nb_2O_5 (99.99 %, Sigma-Aldrich). The starting materials were ground, pressed into a pellet and calcined in an alumina crucible for 10 hrs at 900 °C. The pellet was then reground, pelleted and heated at 1300 °C for 10 hours before being cooled to room temperature at a rate of 5 °C/min. The latter heating step was repeated until a phase pure product was obtained.

X-ray powder diffraction patterns were collected at room temperature on a PANalytical Empyrean Powder diffractometer with Cu $K_{\alpha1}$ radiation. Data were recorded in the range $5° < 2\theta < 70°$, with a step size of 0.0131°. Time of flight (TOF) neutron powder diffraction data were collected at room temperature (~20°C) on the Polaris diffractometer at the ISIS pulsed neutron source, Rutherford Appleton Laboratory, UK. ~ 5g of $Ba_3WNbO_{8.5}$ were loaded into an 8 mm diameter cylindrical vanadium can and data acquired in all 5 detector banks (covering a continuous *d*-spacing range from ~0.2Å < *d* < 25Å) for ~300 µAh integrated proton beam to the ISIS target (corresponding to ~2 hours exposure). The morphology of the sintered pellets was monitored using a scanning electron microscope (SEM) (Carl Zeiss Gemini 300). The sample was covered with a thin layer of sputtered gold.

A pellet of ~ 10 mm diameter was prepared from a powdered sample of $Ba_3WNbO_{8.5}$ and sintered for 10 hours at 1300 °C to achieve ~ 92 % of the theoretical density. Pt electrodes were painted on both sides of the pellet using a Pt-paste (Metalor 6082). Impedance spectroscopy measurements were recorded in the frequency range 0.1 Hz – 1 MHz with a Solartron 1260 impedance analyser. Data were recorded upon cooling from 700 °C to 450 °C in a sealed tube furnace under a dry flow of air, nitrogen, oxygen and 5 % Hydrogen/nitrogen. The impedance data were measured every 15 °C with 2 hours of equilibration time at each temperature. The geometrical factor (the ratio of surface area to thickness of the pellet) was used to correct the data obtained and the data was treated with the ZView software.

Results and Discussion

Preliminary Characterisation

The SEM micrographs (Figure S1) show that the sample exhibits a grain size of ~ 5 – 30 µm. No secondary phases can be detected from backscattered micrographs thus confirming the purity of the synthesised sample. The X-ray diffraction pattern of $Ba_3WNbO_{8.5}$ could be indexed with the space group $R\bar{3}m$ H (giving a = 5.8551(2) Å and c = 20.9884(5) Å).

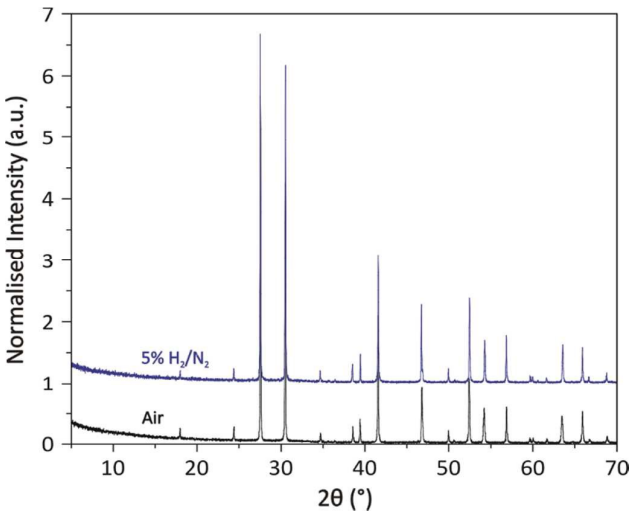

Figure 1. X-ray diffraction patterns of the "as prepared" $Ba_3WNbO_{8.5}$ (black line) and after 24 hours annealing in 5% H2 in N_2 at 600 °C (blue line).

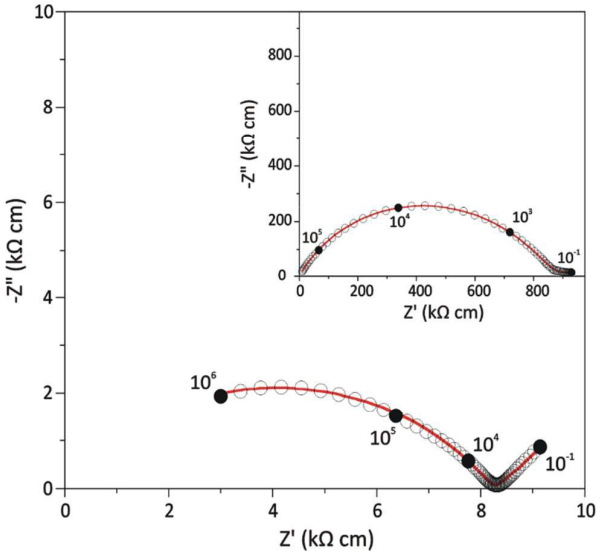

Figure 2 Complex impedance plot recorded in dry air at 625.5 °C. An electrode response is observed in the low frequency region. The inset shows the complex impedance plot recorded in dry air at 450 °C. The numbers and corresponding filled circles indicate selected frequencies (in Hz), while the red line is the equivalent circuit fitting.

This space group has been previously reported for $Ba_3W_{1.33}Nb_{0.66}O_{8.66}$ [20]. There was no evidence of impurities.

X-ray diffraction data were also recorded after $Ba_3WNbO_{8.5}$ was annealed at 600 °C for 24 hours in flowing O_2, N_2 and 5 % H_2/N_2. The X-ray diffraction data show no evidence of

View Article Online
DOI: 10.1039/C7TA08989A

impurities or change in crystal structure post annealing. The X-ray diffraction patterns of a sample of $Ba_3WNbO_{8.5}$ annealed at 600 °C for 24 hours in flowing air and 5 % H_2/N_2 is displayed in Figure 1. This is similar to the $Ba_3MoNbO_{8.5}$ compound which also demonstrates a wide stability range under reducing conditions.

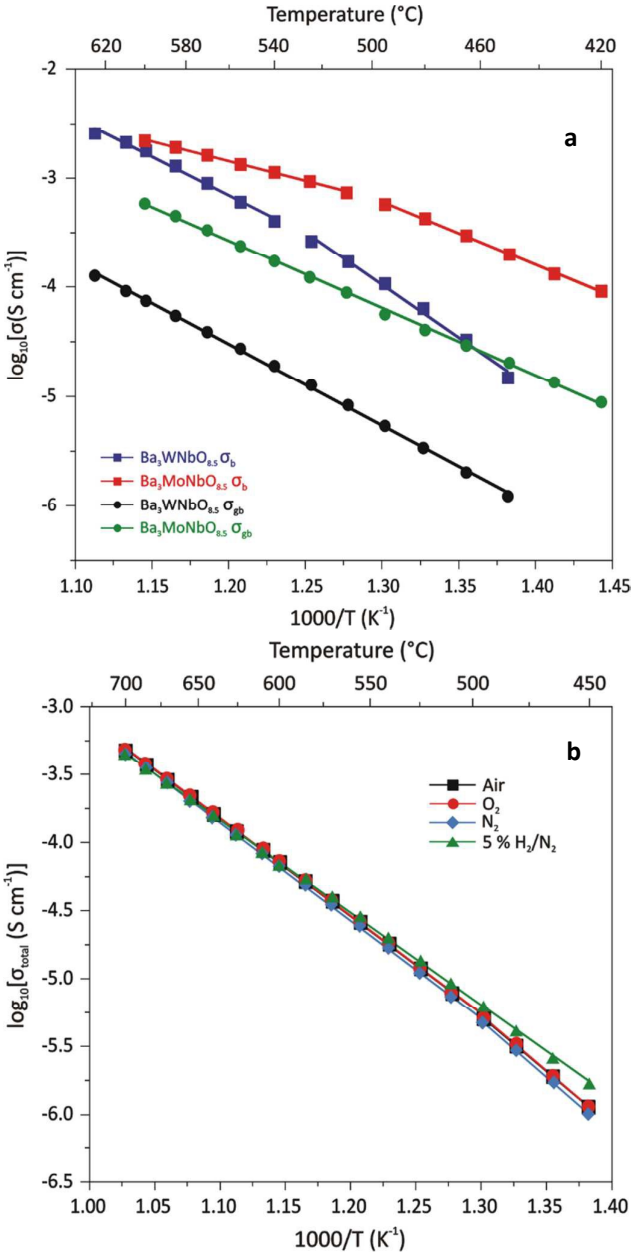

Figure 3 **(a)** Arrhenius plots of the bulk (σ_b) and grain boundary (σ_{gb}) conductivities of $Ba_3WNbO_{8.5}$ and $Ba_3MoNbO_{8.5}$. **(b)** Arrhenius plots of the total conductivities of $Ba_3WNbO_{8.5}$ in a range of different atmospheres. Linear fits to the data are shown.

Electrical Properties

A typical impedance spectrum of $Ba_3MoNbO_{8.5}$ recorded in dry air at 600 °C is presented in Figure 2. An electrode response is observed in the low frequency region (< 10 Hz) at all temperatures above 500 °C, indicative of ionic conduction in a material with partially blocking electrodes. [21] The electrode response was found to become less resistive when the oxygen content of the atmosphere increased, strongly indicating oxide ion mobility.

The bulk and grain boundary responses overlap at higher frequency. Equivalent circuit analysis was performed to extract the individual bulk, grain boundary and electrode responses at each temperature (the model used is displayed in Figure S2). The electrode response could be fit with a short Warburg element indicating finite length diffusion. The bulk and grain boundary responses have respective capacitance values of C_B ~ 6.5 pF cm^{-1} and $C_{Gb,}$ ~ 0.18 nF cm^{-1}.

The Arrhenius plot of the bulk and grain boundary conductivities of $Ba_3WNbO_{8.5}$ and $Ba_3MoNbO_{8.5}$ are presented in Figure 3 (a). For $Ba_3WNbO_{8.5}$ the grain boundaries constitute the most resistive part, thus dominating the total resistivity of the material. The grain boundary conductivity is more than one order of magnitude lower than the bulk conductivity. This could be a result of the grain boundary having different fractional occupancies of O(2) and O(3) or different oxygen stoichiometry than the bulk. The ionic conductivity of $Ba_3MoNbO_{8.5}$ is known to be sensitive to small changes in the fractional occupancies of O(2) and O(3) [19]. The grain boundary conductivity of $Ba_3WNbO_{8.5}$ is 7.5 × 10^{-5} S cm^{-1} at 600 °C with an activation energy of 1.48 ± 0.015 eV. The bulk conductivity is 0.0017 S cm^{-1} at 600 °C. A change in slope is observed at temperatures > 525 °C, with the bulk activation energy lowering from 1.94 eV to 1.40 eV. A similar change in slope has previously been reported for Ba_3MoNbO_8. [18, 19] At 450 °C the bulk conductivity of $Ba_3WNbO_{8.5}$ is approximately an order of magnitude lower than that of $Ba_3MoNbO_{8.5}$. Upon heating the bulk conductivities of $Ba_3WNbO_{8.5}$ and $Ba_3MoNbO_{8.5}$ converge (σ_b = 0.0017 S cm^{-1} and 0.0022 S cm^{-1} for $Ba_3WNbO_{8.5}$ and $Ba_3MoNbO_{8.5}$ respectively).

Figure 3(b) displays the Arrhenius plot of the total conductivity of $Ba_3WNbO_{8.5}$ in a range of different atmospheres. The results suggest that $Ba_3WNbO_{8.5}$ exhibits negligible electronic conductivity over the pO_2 range measured. This is in stark contrast to $Ba_3MoNbO_{8.5}$, where an electronic component to the bulk and grain boundary conductivity is seen in 5% H_2/N_2 [18].

Crystal Structure of $Ba_3WNbO_{8.5}$:

W^{6+} is more stable than Mo^{6+} under reducing conditions and possesses a similar ionic radius (0.59 Å and 0.60 Å for Mo^{6+} and W^{6+} respectively). Upon substituting W^{6+} for Mo^{6+} in the oxide ion conductor $La_2Mo_2O_9$ (LAMOX) the conductivity decreases only very slightly as the W concentration increases. This reduction in the ionic conductivity is observed at all temperatures [22] and demonstrates similar electrical properties for the Mo^{6+} and W^{6+} substituted phases. The slight difference in the ionic conductivity of LAMOX and W^{6+} substituted LAMOX phases are attributed to subtle changes in the crystal structure [22] rather than the different electrical properties of W^{6+} and Mo^{6+}. The bulk conductivity of $Ba_3WNbO_{8.5}$ is an order of magnitude lower than that of $Ba_3MoNbO_{8.5}$ at 450 °C but converges at higher temperatures. Similar behaviour is

View Article Online
DOI: 10.1039/C7TA08989A

observed in $Ba_3Mo_{1-x}Nb_{1+x}O_{8.5-x/2}$ and is a result of a change in M(1), M(2) and O(3) fractional occupancies upon increasing x. A neutron diffraction study of $Ba_3WNbO_{8.5}$ has been performed in order to further investigate differences in the electrical properties and crystal structures of $Ba_3MoNbO_{8.5}$ and $Ba_3WNbO_{8.5}$.

Rietveld refinement was performed using the GSAS/EXPGUI package [23, 24]. Modelling of the background was performed using a shifted Chebyschev polynomial function and the peak shapes were fitted using a Pseudo-Voigt function convoluted with back to back exponentials. $Ba_3W_{1.33}Nb_{0.66}O_{8.66}$ was previously reported as a 9R polytype perovskite, with trimers of $(W/Nb)O_6$ face-sharing octahedra connected by corner-sharing in the stacking sequence $(hhc)_3$ (space group $R\bar{3}m$) [20]. In this model the barium atoms are in position 3*a* (Ba(1)) and 6*c* (Ba(2)). The W and Nb atoms share the 6*c* (W(1)/Nb(1)) and the 3*b* (W(2)/Nb(2)) sites. The oxygen atoms occupy two distinct positions, 18*h* (O(1)) and 9*e* (O(2)). This model is closely related to the hybrid palmierite-9R polytype model proposed for Ba_3MoNbO_8, with the only difference being that the oxygen in position 6*c* (or in the split position 36*i*) is missing. Employing the $Ba_3W_{1.33}Nb_{0.67}O_{8.66}$ model provided acceptable statistical factors (χ^2 = 8.30, R_p = 6.41 % and wR_p = 5.62 %). However, examination of the fitted histograms revealed significant discrepancies between observed and calculated profiles, suggesting the 9R structural model was incorrect.

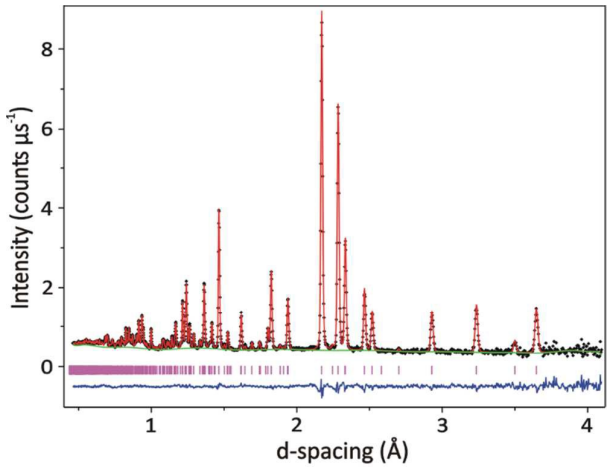

Figure 4 Fitted room temperature TOF powder neutron diffraction pattern from $Ba_3WNbO_{8.5}$ collected in the Polaris 2θ ~ 90° detector bank. Black crosses indicate the observed data, the red line the Rietveld fit, the blue line the difference between the observed and the calculated profiles, the green line the fitted background function and the pink vertical bars mark the reflection positions.

An excellent Rietveld fit was obtained with the hybrid 9R polytype – palmierite model previously reported for $Ba_3MoNbO_{8.5}$ [18] (space group $R\bar{3}m$ H; a = 5.8570(1) Å, c = 20.9964(5) Å, V = 623.77(3) Å^3; χ^2 = 2.37, R_p = 5.75% and R_{Wp} = 3.18%). The Rietveld refinement fit from the neutron diffraction data taken from the 90° detector bank is presented in Fig. 4. The $Ba_3WNbO_{8.5}$ structure is composed of intertwined 9R polytype and palmierite domains, with mixed $(W/Nb)O_4$ tetrahedra and $(W/Nb)O_6$ octahedra (Fig. 5). The different crystal structures reported for $Ba_3WNbO_{8.5}$ and $Ba_3W_{1.33}Nb_{0.67}O_{8.66}$ [20] are potentially a result of the change in stoichiometry. The structural parameters obtained from Rietveld refinement of the $Ba_3WNbO_{8.5}$ neutron diffraction data are tabulated in Table S1.

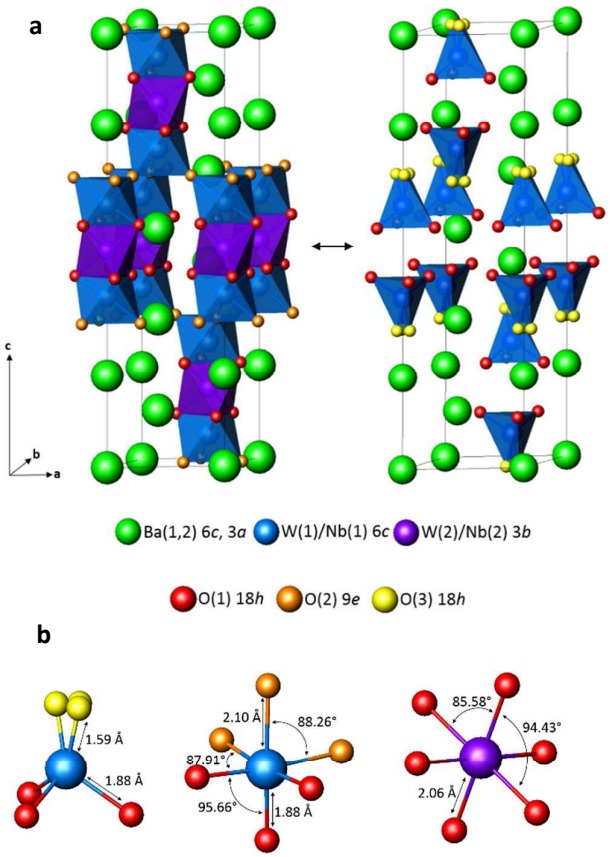

Figure 5. Crystal structure of $Ba_3WNbO8.5$. (a) The hybrid structural model formed by the superimposition of the 9R-polytype (left) and the palmierite (right) sub-units representing the average structure of the system. (b) Bond lengths and angles of the (W/Nb)O4 tetrahedra and (W/Nb)O6 octahedra. Colours in (a) and (b) indicate: green Ba(1)/Ba(2), blue W(1)/Nb(1), purple W(2)/Nb(2), red O(1), orange O(2) and yellow O(3).

Anisotropic atomic displacement parameters were refined for all atoms. Disorder of the oxygen atom, O(3), within the $(Mo/Nb)O_4$ tetrahedra was evidenced by large U_{11}, U_{22}, and U_{12} values. This was modelled by using a single isotropic U factor for O(3) and splitting the site as shown in Table S1 and Figure 5. The disorder of O(3) onto the 18*h* positions arises as a result of the short distance between Ba(2) and W(1)/Nb(1) so that the disorder stabilizes the structure, resulting in longer and more realistic Ba(2)–O(3) and W(1)/Nb(1)–O(3) bond lengths. Similar structural disorder has been reported for $Ba_3MoNbO_{8.5}$ [18] and the mixed conducting hexagonal

View Article Online
DOI: 10.1039/C7TA08989A
Journal Name ARTICLE

perovskite $Ba_7Y_2Mn_3Ti_2O_{20}$ [25]. The thermal ellipsoids of O(1), O(2), Ba and W/Nb atoms are displayed in Table S1. The W/Nb cations exhibit highly anisotropic thermal displacement along the *c*-axis in both the 6*c* and 3*b* sites (Table S1) Similar U_{ij} values have been found for Mo/Nb in $Ba_3MoNbO_{8.5}$, and have been ascribed to the different coordination environments of the Mo/Nb cations.

The Ba fractional occupancies refined to within ±1 % of the full occupancy and thus were fixed in further refinement at 1.0. Refinement of the individual oxygen site occupancies resulted in an overall oxygen stoichiometry of 8.5. The oxygen (O(1)) at position 18*h* is fully occupied while the O(2) and O(3) sites are partially occupied. The results demonstrate that the replacement of Mo^{6+} with W^{6+} is accompanied by large changes in the fractional occupancies of O(2), O(3), M(1) and M(2). At room temperature the majority of the W(1)/Nb(1) ions in $Ba_3WNbO_{8.5}$ exhibit octahedral coordination with just ~ 13 % of W(1)/Nb(1)O_4 tetrahedra within the average structure. In contrast there are ~ 50% Mo(1)/Nb(1)O_4 tetrahedra within the average structure of $Ba_3MoNbO_{8.5}$ [19]. The W^{6+} preferentially occupies the M(2) site so that there is an increase in the fractional occupancy of the M(2) site upon replacement of Mo^{6+} with W^{6+} (Table S1). It has previously been reported that there is a strong correlation between the oxide ionic conductivity and the number of (Mo/Nb)O_4 tetrahedra within the average structure of $Ba_3MoNbO_{8.5}$. The magnitude of oxide ionic conductivity observed is enhanced as the ratio of (Mo/Nb)O_4 tetrahedra to (Mo/Nb)O_6 octahedra increases. Oxide ion migration occurs via the partially occupied O(2) and O(3) sites in $Ba_3MoNbO_{8.5}$. The increase in the number of (Mo/Nb)O_4 tetrahedra most likely offers more low energy transition paths for transport of the O^{2-} ions enhancing the conductivity [19]. The ratio of (Mo/Nb)O_4 tetrahedra to (Mo/Nb)O_6 octahedra strongly decreases upon replacement of W^{6+} for Mo^{6+} so that the ionic conductivity is an order of magnitude lower in $Ba_3WNbO_{8.5}$ at 450 °C (Figure 3(a)).

However upon heating, the bulk ionic conductivities of $Ba_3WNbO_{8.5}$ and $Ba_3MoNbO_{8.5}$ converge (Fig. 3(a)) so that by 600 °C similar ionic conductivities are observed for both compounds. A similar result has been reported for the $Ba_3Mo_{1-x}Nb_xO_{8.5-x/2}$ solid solution. [26] A variable temperature neutron diffraction study of $Ba_3MoNbO_{8.5}$ has previously shown that above 300 °C the oxygen/vacancy distribution changes as the temperature increases so that the ratio of (Mo/Nb)O_4 tetrahedra to (Mo/Nb)O_6 octahedra increases upon heating with a concomitant increase in the ionic conductivity [19]. A change in slope is evidenced in the Arrhenius plot of both $Ba_3WNbO_{8.5}$ and the $Ba_3MoNbO_{8.5}$ at 540 °C and 510 °C respectively.

The variable temperature neutron diffraction study of $Ba_3MoNbO_{8.5}$ demonstrated that above ~ 500 °C the rate of change in the ratio of (Mo/Nb)O_4 tetrahedra to (Mo/Nb)O_6 octahedra slows down. [19] The gradient of the Arrhenius plot of the bulk conductivity of $Ba_3WNbO_{8.5}$ above 540 °C is greater than that observed for $Ba_3MoNbO_{8.5}$. This indicates that above 540 °C there is a larger rate of increase in the number of tetrahedra within the crystal structure of $Ba_3WNbO_{8.5}$. A likely explanation for the convergence of the ionic conductivity at 600 °C is therefore that the same structural rearrangement of (M/Nb)O_4 tetrahedra and (M/Nb)O_6 octahedra occurs in $Ba_3MNbO_{8.5}$ (M = Mo and W) upon heating but the rate of change in the number of tetrahedra above ~500 °C is greater for M = W^{6+} and by 600 °C the number of (M/Nb)O_4 tetrahedra within the average structure of $Ba_3MNbO_{8.5}$ (M = Mo and W) are at similar levels. The same result is observed for the $Ba_3Mo_{1-x}Nb_xO_{8.5-x/2}$ solid solution [26] and suggests that the structure of the hexagonal perovskite derivative $Ba_3MNbO_{8.5}$ has the propensity to rearrange to an optimum ratio of (M/Nb)O_4 tetrahedra and (M/Nb)O_6 octahedra upon heating to 600 °C. Variable temperature neutron diffraction are warranted to investigate this further.

Selected bond lengths and angles of $Ba_3MoNbO_{8.5}$ and $Ba_3WNbO_{8.5}$ are displayed in Supplementary Tables S2 and S3 for comparison purposes. The structure of $Ba_3MNbO_{8.5}$ (M = Mo, W) contains three equal M(1)–O(1) bonds and three equal O(1)–M(1)–O(1) angles (α) forming the M(1)$O(1)_3$ unit, which is common to the M(1)–$O(1)_3$O(3) tetrahedron and the M(1)–$O(1)_3O(2)_3$ octahedron. M(1)–$O(1)_3$O(3) is then defined by the M(1)–O(3) distance and the O(1)–M(1)–O(3) angle (β), obtained by the average of the possible angles given by the O(3) split positions. The M(1)–$O(1)_3O(2)_3$ octahedron is defined by the M(1)–O(1) bond length, α, the M(1)–O(2) bond lengths and the O(1)–M(1)–O(2) and O(2)–M(1)–O(2) angles (γ and δ respectively) (Figure S3). Upon replacement of W^{6+} for Mo^{6+} there are clear changes to the bond lengths and angles of the M(1)O_x polyhedra. The M(1)-O(1) bond length increases whereas the M(1)-O(2) and M(1)-O(3) bond lengths both decrease in magnitude. The angle α decreases whereas the angles β, γ and δ increase. These changes reflect the relaxation of the structure as the number of oxygen vacancies at the O(3) site increases. The changes of the bond lengths and angles demonstrate that the replacement of W^{6+} for Mo^{6+} leads to displacement of the M(1) atom closer to the O(2)/O(3) sites, in respect to its equilibrium position in $Ba_3MoNbO_{8.5}$, with subsequent relaxation of the surrounding lattice (Table S2). The magnitude of the displacement can be obtained from the distance between M(1) and the [O(1)-O(1)-O(1)] face, given by D = –(M(1)–O(1))cos(β) [19].

Displacement of the metal atoms adjacent to the mobile oxygen sites has been reported in various oxide ion conductors [27, 28] and can be associated with the energetics of the ionic transport as displacement of *d*-metal cations from oxygen vacancies is thought to lower the motional enthalpy required for the mobility of the oxide ions [29]. The motional enthalpy, ΔH_m, directly contributes to the activation energy of the conduction process and is the sum of two components: a barrier energy for the ionic hopping and a relaxation energy needed for the lattice relaxation around the conductive sites [30]. The M(1) polyhedra in $Ba_3MoNbO_{8.5}$ are already distorted [18] and it has been previously reported that the M(1) displaces away from the O^{2-} ions at the O(2)/O(3) sites upon heating above 300 °C [19]. Upon substituting W^{6+} for Mo^{6+} the M(1) atom shifts in the opposite direction, i.e. towards the O(2) and O(3) positions. Such motion of M(1) towards the partially occupied

View Article Online
DOI: 10.1039/C7TA08989A

oxygen sites results in the increase of the bulk activation energy from 1.21 eV for $Ba_3MoNbO_{8.5}$ to 1.94 eV for Ba_3WNbO_8 as more energy is needed for the relaxation of the metal lattice around the oxygen vacancies and the O(2)/O(3) sites.

Out-of-centre distortions in the coordination polyhedra of d^0 transition metals are also influenced by electronic effects, which mutually contribute to the overall displacement [31]. Electronic distortions, such as second order Jahn-Teller distortions, are generated in the presence of transition metals with large formal charges and small cationic radii. A decrease in the second order Jahn-Teller effect would be expected upon substituting W^{6+} for Mo^{6+}since W^{6+} is a moderate distorter, while Mo^{6+} is a strong distorter. [32] The M(1) displacement towards the O(2)/O(3) sites evidenced for $Ba_3WNbO_{8.5}$ with respect to the M(1) "equilibrium" position in $Ba_3MoNbO_{8.5}$ is hence a result of both the electronic and structural effects induced by the substitution of W^{6+} for Mo^{6+}.

Conclusions

In summary the electrical and structural properties of the novel oxide ion conductor $Ba_3WNbO_{8.5}$ have been elucidated. W^{6+} is more stable than Mo^{6+} under reducing conditions so that replacing W^{6+} for Mo^{6+} reduces the electronic component in low pO_2. This is similar to tungsten doping studies of LAMOX where the presence of W^{6+} leads to an increase in the stability range for $La_2Mo_{0.5}W_{1.5}O_9$ at 800 °C. [32]

In $Ba_3MNbO_{8.5}$ (M = Mo, W) the ionic migration is thought to proceed via tetrahedral and octahedral interchange occurring through a cooperative interstitialcy-like motion of the oxygen atoms between the occupied and vacant oxygen sites within the pseudo-cubic $BaO_{2.5}$ layers. At 20 °C in $Ba_3WNbO_{8.5}$, the O(3) site presents a much lower fractional occupancy than observed for $Ba_3MoNbO_{8.5}$ thus reducing the concentration of charge carriers, resulting in a bulk oxide ionic conductivity an order of magnitude lower than that reported for $Ba_3MoNbO_{8.5}$ at 450 °C. Upon heating to 600 °C the bulk conductivities of $Ba_3MoNbO_{8.5}$ and $Ba_3WNbO_{8.5}$ converge. Given that the ionic conductivity has been shown to be sensitive to the ratio of $(M/Nb)O_4$ tetrahedra to $(M/Nb)O_6$ tetrahedra [19, 26], it's highly likely that the crystal structure of $Ba_3MNbO_{8.5}$ hexagonal perovskite derivatives rearranges to an optimal ratio of tetrahedra:octahedra upon heating. Finally the results demonstrate that oxide ion conductivity can be established in other members of the $Ba_3MM'O_{8.5}$ family and the synthesis of new materials where M = a hexavalent cation and M' = a pentavalent cation could result in new materials with applications as SOFC electrolytes, oxygen sensors and/or oxygen separation membranes.

Conflicts of interest

There are no conflicts to declare.

Acknowledgements

This research was supported by the Northern Research Partnership and the University of Aberdeen. We also acknowledge Science and Technology Facilities Council (STFC) for provision of beamtime at ISIS.

References

1 B. C. H. Steele, Materials Science and Engineering: B, 1992, **13**, 79-87.
2 J. B. Goodenough, *Annu. Rev. Mater. Res.*, 2003, **33**, 91-128.
3 L. Malavasi, C. A. J. Fisher and M. S. Islam, *Chem. Soc. Rev*., 2010, **39**, 4370-4387.
4 S. J. Skinner and J. A. Kilner, *Materials Today*, 2003, **6**, 30-37.
5 O. Yamamoto, *Electrochim. Acta,* 2000, **45**, 2423-2435.
6 E. D. Wachsman and K. T. Lee, *Science*, 2011, **334**, 935-939.
7 S. C. Singhal, *Solid State Ionics*, 2000, **135**, 305-313.
8 A. Navrotsky, *J. Mater. Chem*., 2010, **20**, 10577-10587.
9 P. Lacorre, F. Goutenoire, O. Bohnke, R. Retoux and Y. Laligant, *Nature*, 2000, **404**, 856-858.
10 N. M. Sammes, G. A. Tompsett, H. Näfe and F. Aldinger, *Journal of the European Ceramic Society*, 1999, **19**, 1801-1826.
11 E. Kendrick, M. S. Islam and P. R. Slater, *J. Mater. Chem*., 2007, **17**, 3104-3111.
12 T. Ishihara, H. Matsuda and Y. Takita, *J. Am. Chem. Soc*., 1994, **116**, 3801-3803.
13 M. Li, M. J. Pietrowski, R. A. De Souza, H. Zhang, I. M. Reaney, S. N. Cook, J. A. Kilner and D. C. Sinclair, *Nat Mater*, 2014, **13**, 31-35.
14 K. Fujii, Y. Esaki, K. Omoto, M. Yashima, A. Hoshikawa, T. Ishigaki and J. R. Hester, *Chem. Mater*. 2014, **26**, 2488–2491.
15 K. T. Lee, H. S. Yoon and E. D. Wachsman, *Journal of Materials Research*, 2012, **27**, 2063-2078.
16 K. R. Kendall, C. Navas, J. K. Thomas and H. Z. Loye, *Solid State Ionics*, 1995, **82**, 215-223.
17 J. W. Fergus, *J. Power Sources*, 2006, **162**, 30-40.
18 S. Fop, J. M. S. Skakle, A. C. McLaughlin, P. Connor, J. T. S. Irvine, R. I. Smith and E. J. Wildman, *J. Amer. Chem. Soc*., 2016, **138**, 16764-16769.
19 S. Fop, E. J. Wildman, J. T. S. Irvine, P. A. Connor, J. M. Skakle, C. Ritter and A. C. McLaughlin, *Chem. Mater*., 2017, **29**, 4146-4152.
20 S. Kemmler-Sack and U. Treiber, *Zeitschrift fuer Anorganische und Allgemeine Chemie*, 1981, **478**, 198-204.
21 J. T. S. Irvine, D. C. Sinclair, A. R. West, *Adv. Mater.* 1990, **2**, 132-138.
22 S. Georges , O. Bohnké , F. Goutenoire , Y. Laligant , J. Fouletier , P. Lacorre, *Solid State Ionics*, 2006, **177**, 1715–1720.
23 A. C. Larson and R. B. Von Dreele, Los Alamos National Laboratory Report LAUR 86-748 (1994).
24 B. H. Toby, *J. Appl. Cryst*., 2001, **34**, 210-213.
25 X. Kuang, M. Allix, R. M. Ibberson, J. B. Claridge, H. Niu and M. J. Rosseinsky, *Chem. Mater*. 2007, **19**, 2884-2893.
26 S. Fop, E. J. Wildman, J. M. S. Skakle, C. Ritter and A. C. Mclaughlin,. *Inorganic Chemistry,* 2017, **56**, 10505-10512.
27 M. S. Islam, *J. Mater. Chem*., 2000, **10**, 1027-1038.
28 M. S. Islam, J. R. Tolchard and P. R. Slater, *Chem. Commun*., 2003, **13**, 1486-1487.
29 J. B. Goodenough, A. Manthiram, M. Paranthamam and Y. S. Zhen, *Mat. Sci. Eng. B-Solid*, 1992, **B12**, 357-364.
30 J. B. Goodenough, *Annu. Rev. Mater. Res*., 2003, **33**, 91-128.
31 M. Kunz and D. I. Brown, *J. Solid State Chem*., 1995, **115**, 395-406.

View Article Online
DOI: 10.1039/C7TA08989A

32 K. M. Ok, P. S. Halasyamani, D. Casanova, M. LLunell, P. Alemany and S. Alvarez, *Chem. Mater*., 2006, **18**, 3176-3183.
33 D. Marrero-Lopez, J. Canales-Vazquez, J. C. Ruiz-Morales, J. T. S. Irvine and P. Nunez, *Electrochimica Acta*, 2005, **50**, 4385-4395.

View Article Online
DOI: 10.1039/C7TA08989A

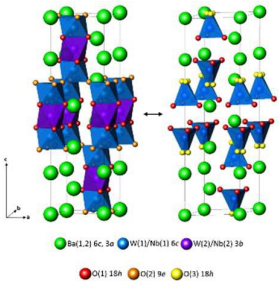

The crystal structure of the novel oxide ion conductor $Ba_3WNbO_{8.5}$.